Comparative analysis of selective area grown Ga- and N-polar InGaN/GaN nanowires for quantum emitters ⊘

Arnob Ghosh ; Kamruzzaman Khan ; Shrivatch Sankar ; Zhe (Ashley) Jian ; Syed M. N. Hasan ;
Elaheh Ahmadi ; Shamsul Arafin ✉

Check for updates

CrossMark

View Online

Export Citation

Comparative analysis of selective area grown Ga- and N-polar InGaN/GaN nanowires for quantum emitters ⓔⓟ

View Online   Export Citation   CrossMark

Arnob Ghosh,[1] ⓘ Kamruzzaman Khan,[2] ⓘ Shrivatch Sankar,[1] ⓘ Zhe (Ashley) Jian,[2] ⓘ Syed M. N. Hasan,[3] ⓘ
Elaheh Ahmadi,[2] ⓘ and Shamsul Arafin[1,a] ⓘ

AFFILIATIONS

[1] Department of Electrical and Computer Engineering, The Ohio State University, Columbus, Ohio 43210, USA
[2] Department of Materials Science and Engineering, University of Michigan, Ann Arbor, Michigan 48109, USA
[3] National Renewable Energy Laboratory, Golden, Colorado 80401, USA

[a] Author to whom correspondence should be addressed: arafin.1@osu.edu

ABSTRACT

In this paper, we report the molecular beam epitaxy-grown InGaN-quantum disks embedded within selective area epitaxy of GaN nanowires with both Ga- and N-polarities. A detailed comparative analysis of these two types of nanostructures is also provided. Compared to Ga-polar nanowires, N-polar nanowires are found to exhibit a higher vertical growth rate, flatter top, and reduced lateral overgrowth. InGaN quantum disk-related optical emission is observed from nanowires with both polarities; however, the N-polar structures inherently emit at longer wavelengths due to higher indium incorporation. Considering that N-polar nanowires offer more compelling geometry control compared to Ga-polar ones, we focus on the theoretical analysis of only N-polar structures to realize high-performance quantum emitters. A single nanowire-level analysis was performed, and the effects of nanowire diameter, taper length, and angle on guided modes, light extraction, and far-field emission were investigated. These findings highlight the importance of tailoring nanowire geometry and eventually optimizing the growth processes of III-nitride nanostructures.

One-dimensional nanostructures based on III-nitrides have gained much attention as a promising platform for various applications, including optoelectronics,[1] photocatalysis,[2,3] power electronics,[4] and sensing,[5,6] because they exhibit a significantly lower defect density compared to their planar counterparts.[7–9] In particular, InGaN quantum dots (QDs) and quantum disks (Qdisks) embedded in III-nitride nanowire (NW) structures offer versatility, serving not only as classical optoelectronic devices but also as sources of single photons in quantum devices[10–14] and potentially entangled photon pairs as critical enablers for quantum applications.[15–17]

Plasma-assisted molecular beam epitaxy (PAMBE) has emerged as a popular technique for III-nitride NW growth through self-assembly under nonequilibrium conditions. Self-assembled NWs are grown on low-cost foreign substrates, such as Si, AlN buffer on Si, SiC, and sapphire.[18–22] However, self-assembled NWs suffer from random nucleation and inhomogeneities in indium incorporations in Qdisks.[23–25] Due to the randomness and spontaneity in nucleation, tailoring these NWs by controlling their size, shape, position, and density poses substantial challenges. Meanwhile, selective area epitaxy (SAE) provides an attractive alternative for overcoming these challenges. By employing the SAE technique, it is possible to achieve defect-free NW arrays with precise control over their microstructural properties, composition, spatial homogeneity, as well as diameters and spacings of the NWs.[26–33]

III-nitride surfaces can be terminated either with metal (Ga/In/Al) or with nitrogen (N) atoms, which classifies the materials as metal-polar or N-polar. Such a "crystal face polarity" has important roles in the growth, fabrication, material properties, and device performance. Recent advancements confirm that N-polar structures possess notable performance benefits compared to their

Ga-polar counterparts. By growing N-polar III-nitrides at higher temperatures, the formation of point defects, detrimental for achieving highly efficient emission in the visible range, is significantly reduced.[34] In addition, more efficient indium incorporation can be achieved during the growth of (In,Ga)N along the N-polar direction, thanks to the higher thermal dissociation limit of N-polar InN.[35,36] Furthermore, it has been demonstrated that N-polar GaN/AlGaN NWs exhibit a higher selectivity, verticality, a flat top surface, as well as reduced lateral growth and enhanced vertical growth.[37,38] Research also indicates that N-polar InGaN LEDs may experience reduced electron overflow, making them suitable for high-power operation.[38,39] In addition, N-polar III-nitride nanostructures can be grown under N-rich epitaxy conditions, facilitating efficient p-type conduction by suppressing the formation of defects related to N vacancies.[40,41]

There have been a few demonstrations of N-polar GaN NWs of foreign substrate[26,42–45] by PAMBE using an AlN interlayer. These NWs exhibited defects generated from Al–Si eutectic formation and inversion domains.[43] In particular, the larger diameter NWs showed interior voids and irregular facets.[42] It has recently been demonstrated that GaN NWs with such void-free and smooth facets were grown by switching to N-polar GaN substrates under metal-rich conditions.[37] Despite these studies, a comprehensive analysis of the growth dynamics, the optical properties from InGaN Qdisks in such faceted N-polar GaN NWs, and their comparison with Ga-polar structures are still lacking.

In this work, we report the selective growth of GaN NWs with embedded InGaN Qdisks on both Ga- and N-polar GaN-on-sapphire templates. A detailed comparative analysis of the PAMBE-grown Ga- and N-polar NWs is then provided by performing morphological and spectroscopic characterizations. It is found that NWs grown on N-polar GaN show better control over geometry, such as high vertical growth and reduced lateral growth rates and a flat top instead of hexagonal facet compared to Ga-polar. In order to show the importance of NW geometry control, we analyze the extraction efficiency and emission profile of a single NW-based quantum emitter through numerical simulations. The effects of NW diameter on guided modes, light extraction, and inhibition of leaky emission were also theoretically examined. Our work connects the theoretical discussion based on electromagnetic simulations with the experimental results by considering the experimentally observed geometrical advantages in N-polar NWs. This confirms the N-polar NW as one of the promising waveguide candidates for future quantum emitters.
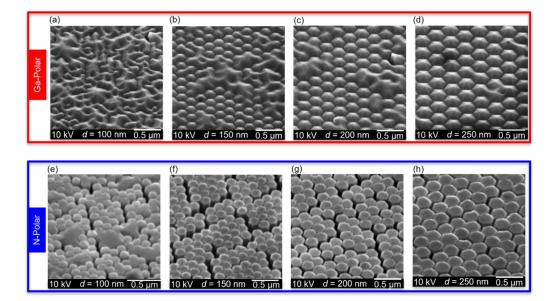
Ga-polar and N-polar GaN-on-sapphire templates were used for SAE of NWs. The template and sample patterning details can be found elsewhere.[37] All samples were grown at the same time under identical conditions using a Veeco GENxplor MBE system. Active nitrogen was supplied by 0.3 SCCM of 99.9995% pure N_2 using a Veeco RF plasma source powered at 350 W. The patterned substrate with a 10 nm Ti mask was first nitrided *in situ* at 400 °C for 10 min to avoid crack formation in the Ti mask during growth. GaN was then grown at 820 °C for 6 h using Ga beam equivalent pressure (BEP) of 2×10^{-7} Torr and the plasma condition mentioned above temperature. The growth temperature was increased by 10 °C to improve the selectivity of the long NWs' growth. Under optimized conditions, with a specific substrate temperature and Ga flux, the epitaxy of GaN was suppressed on the surface of the Ti

mask due to the high desorption rate of Ga adatoms, thereby allowing for growth only in the mask openings. The substrate temperature was then decreased to 600 °C, and ~3 nm InGaN was grown under metal-rich growth conditions. The InGaN was capped by a low-temperature GaN layer before the growth temperature was raised to 820 °C. After the temperature was stabilized at 820 °C for 15 min, GaN was again grown for 6 h under the growth conditions described above. No dopants were introduced during the growth. The temperatures reported here were measured using a thermocouple attached to the substrate.

Figure 1 presents the SEM images of Ga-polar (a)–(d) and N-polar (e)–(h) GaN NWs with varying mask opening diameters d and pitches p (center-to-center spacing). The NW growth details can also be found in Ref. 37. Examining the SEM images reveals that the homogeneity of Ga-polar NWs diminishes with decreasing diameter. The NWs with a diameter of 100 nm [Fig. 1(a)] are fully coalesced. While some instances of coalescence are observed in NWs with larger diameters [Figs. 1(b)–1(d)], the coalesced area remarkably decreases as the diameter increases. In contrast, N-polar NWs are of uniform dimensions across all diameters ranging from 150 to 200 nm [Figs. 1(f)–1(h)]; only NWs with 100 nm diameter [Fig. 1(e)] show some degrees of coalescence. These phenomena are explained by examining the growth rate differences in NWs of varying size and polarity.

Figure 2(a) schematically illustrates the representative N-polar and Ga-polar NWs under study. Figures 2(b) and 2(c) show the 45° tilted SEM images that reveal the height difference of NWs with a 250 nm mask opening and 300 nm pitch. The average height and diameter of the NWs were calculated from the SEM data of NWs with various mask openings, and the results are then plotted as shown in Figs. 2(d) and 2(e). The height of the NWs was measured from the bottom by taking into account the correction factor associated with the tilt angle. For accurately measuring the NW diameters, the coalesced areas of the samples were avoided. Although the Ga- and N-polar samples were grown at the same time under identical conditions, the N-polar NWs are observed to be nearly twice as tall as the Ga-polar ones. This suggests that the N-polar NWs inherently experience a higher vertical growth rate, nearly double that of Ga-polar NWs.

Interestingly, the lateral growth rate of Ga-polar NWs was found to be higher compared to N-polar NWs, especially for smaller mask openings (<150 nm), where the NW diameter exceeded the mask opening size, leading to the coalescence. Conversely, the diameter of N-polar NWs closely matches the target mask opening size especially for opening sizes greater than 100 nm and no coalescence was observed for these NWs. As the diameter of the openings increases, the ratio between mask opening and pitch also increases, which leads to a reduction in total available Ga atoms per opening. This results in the lowering of the NW growth rate in both vertical and lateral directions with increasing mask opening. Due to this reduction in the lateral growth rate, the degree of coalescence also reduces with increasing mask opening diameter in the case of both polarities.

From the SEM images of Fig. 1, it is evident that the N-polar NWs exhibit flat top surfaces, while the Ga-polar NWs display a pyramidal structure on their top surfaces, akin to the previous reports on self-assembled and SAE of GaN NWs.[46] The distinctions observed between Ga-polar and N-polar NW growth can be

FIG. 1. 45°-titled SEM images of the as-grown (a)–(d) Ga-polar and (e)–(h) N-polar GaN NWs with different diameters d and pitches p. Here, (a) and (e) p = 150 nm, (b) and (f) p = 200 nm, (c) and (g) p = 250 nm, and (d) and (h) p = 300 nm.
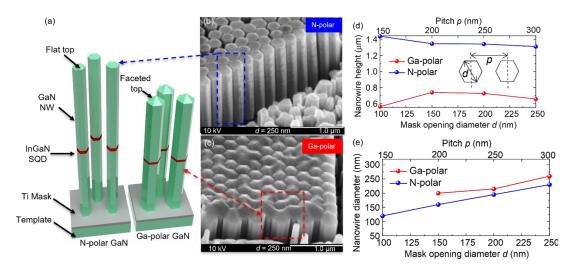

FIG. 2. (a) Schematic of the Ga-polar and N-polar NWs, 45°-titled SEM images of the (b) N-polar and (c) Ga-polar NW samples with 250 nm mask opening, and a comparison between N-polar and Ga-polar NWs in terms of (d) NW height vs mask opening diameter and (e) NW diameter vs mask opening diameter.

comprehended from a thermodynamic standpoint by considering the surface energy values associated with different crystal planes. Under thermodynamic equilibrium, the shape of a crystal is determined by the configuration that minimizes the total surface energy while maintaining its volume. Based on the broken-bond model[46,47] and *ab initio* calculations,[48] it has been established that the surface energy of GaN planes follows the order: m (non-polar) $\leq a$ (non-polar) $\approx \bar{c}$ (polar) $< r$ (semipolar) $\ll c$ (polar). For Ga-polar NWs, growth occurs along the c plane, specifically in the [0001] direction, where the sidewalls are stabilized by the lowest energy

m- and a-planes. Since the semipolar r plane possesses a lower surface energy (almost half) compared to the polar c plane, the top surface is formed by stable semipolar planes terminating at the sidewalls, resulting in a pyramid-shaped faceted top surface. This observation is further supported by the presence of deep cusps along the $\langle 10\bar{1}n \rangle$ directions in the kinetic Wulff's plot, specifically along the [0001] direction.[47,49]

Meanwhile, the growth of N-polar NWs takes place along the $\bar{c}$ plane, specifically in the [000$\bar{1}$] direction. In this case, the sidewalls are also stabilized by the lowest energy m- and a-planes, but the
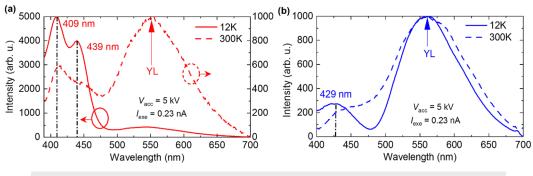
FIG. 3. CL spectra of (a) Ga-polar and (b) N-polar NWs measured at a constant beam current. YL: yellow luminescence.

formation of semipolar planes along the top surface is precluded due to the fact that the polar $\bar{c}$ plane possesses a lower surface energy than the semipolar planes. Consequently, the top surface of N-polar NWs remains flat formed by the $\bar{c}$ plane instead of exhibiting a pyramid-shaped facet. This observation is further supported by the presence of deep cusps in the $\langle 1\bar{1}00 \rangle$ and $[000\bar{1}]$ directions in the kinetic Wulff's plot along the $[000\bar{1}]$ direction.[47,49] It has also been suggested that the growth rate along the pyramid-shaped r-plane is slower, which may explain the lower vertical growth rate of Ga-polar NWs compared to N-polar NWs.[33]

To investigate the optical emission properties, the NW samples were further analyzed using cathodoluminescence (CL) measurements. Figure 3 shows the CL spectra of the NW samples of both polarities having a diameter of 200 nm and a pitch of 250 nm. The NW structures were excited from top with a spatial resolution of 500×500 nm^2, ensuring that only the response from 2 to 3 NWs was recorded. Furthermore, SEM imaging was used to ensure that the nanowires under excitation were not coalesced. The spectrum of a Ga-polar sample at 12 K is shown in Fig. 3(a), which shows two prominent peaks at 409 and 439 nm. Even at room temperature, multiple peaks were observed, and the peak positions were evaluated by fitting them by Lorentzian curves as shown in Fig. S1 of the supplementary material. Room temperature photoluminescence (PL) was performed, which also reveals a bimodal emission from these NWs (see Fig. S2 of the supplementary material). According to previous reports, strong indium clustering gives rise to multiple emission peaks, and based on that, we believe that the higher energy peak originates from the Qdisk and the lower energy peak is from the indium clustering.[50–53] An estimated indium composition of 9% is associated with the peak at 409 nm, which was calculated using Vegard's law with a bowing parameter of 1.8,[54] without considering the associated polarization charge.

From the N-polar NWs, only the single peak at a longer wavelength 429 nm was observed, as shown in Fig. 3(b). This suggests a higher indium incorporation in the N-polar Qdisk,[35] corresponding to an indium composition of 13%. In addition, the absence of multiple emission peaks indicates that the indium clustering was greatly reduced by switching the polarity from Ga to N. However, the intensity of the emission from N-polar samples is much lower compared to Ga-polar ones, which suggests the presence of an efficient nonradiative recombination channel within the N-polar

Qdisks. Similar luminescence quenching has previously been reported in N-polar InGaN quantum wells (QWs) grown via PAMBE under metal-rich conditions. This quenching is likely attributed to a significant concentration of nonradiative point defects situated at the interfaces between quantum wells (QWs) and barriers, as reported in previous reports.[55,56] We anticipate similar reasons for the lack of Qdisk luminescence in our N-polar NWs, as the growth conditions involved a comparable metal-rich environment. Further growth optimization is required to address this issue of suboptimal luminescence. In addition, from room temperature CL [see Fig. 3(b)] and PL (see Fig. S3 of the supplementary material), a low emission intensity was recorded as the emission peak becomes wider and shifts to longer wavelengths due to thermal effects and merges with yellow defect-related emission often termed yellow luminescence (YL). Although the emission intensity from N-polar Qdisk is comparatively low, they show promise in terms of achieving longer wavelength and single emission peak as well as better geometry control, such as a higher vertical growth rate and reduced lateral overgrowth on the mask.

To delve into the importance of controlling NW geometry, we theoretically assessed the influence of NW diameters and lengths on light emission and extraction at the individual NW level. Numerical calculations were carried out to investigate the emission process from NWs using the finite difference time domain (FDTD) method with a commercial simulation program from Ansys Lumerical Inc. The boundary of the simulation region was surrounded by perfectly matching layers (PMLs), and the mesh size was kept below $\lambda/20 \times n$, where n is the refractive index of GaN. A finite difference mode solver, which provides both effective refractive indices and the field distribution of the guided modes, was used for investigating the guiding properties of the NW. To simulate the QDs, an in-plane point electric dipole source radiating at wavelength $\lambda = 450$ nm was placed at the NW axis, 0.5 μm apart from the NW base. While running numerical simulations, the NW polarity was not considered as the materials with either polarity exhibit similar refractive indices.

We first simulated a single cylindrical NW with a diameter of 200 nm and a length of 1 μm. This NW contains a QD positioned at its central axis. Figure 4(a) illustrates the normalized far-field emission profile, represented by the red curve, which notably deviates from a Gaussian profile. We computed the light
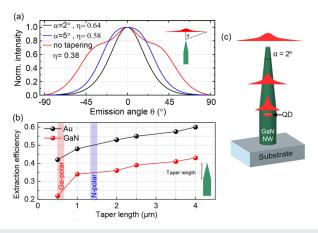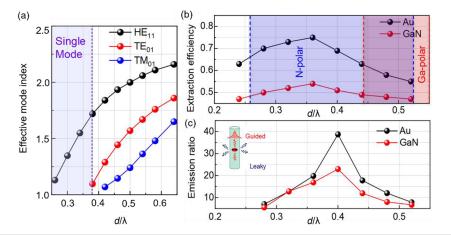
FIG. 4. Effects of the tapered tip on light emission. (a) Normalized far-field emission profile for different taper angles. (b) η at the nanowire end as a function of vertical length of the tapered portion for two different substrates, GaN and Au. (c) Schematic of the mode expansion in a tapered GaN NW.
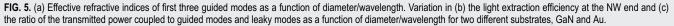
extraction efficiency η as 0.38, determined as the ratio of radiation power in the vertical direction from the NW's top [with a numerical aperture (NA) of 0.7] to the total power injected into the simulation via the electric dipole source. The primary cause for this suboptimal η lies in the unfavorable far-field emission profile.

For effectively directing light emanating from the NW's ends, the strategic tapering of the NW's tip proves advantageous.[57] Tapering ensures a smooth reduction in the effective refractive index and gradually expands the fundamental mode as depicted in Fig. 4(c), which results in a reduction in the reflection at the semiconductor–air interface and in the far-field emission angle. The effects of tapering angle were systematically explored in the simulation. The introduction of a tapering angle $\alpha = 5°$ results in a narrower Gaussian far-field emission, represented by the blue curve in Fig. 4(a). This leads to a significant enhancement in the extraction

efficiency, reaching 0.58. A further reduction of α to 2° results in an even narrower Gaussian far-field emission profile along with an increased η of 0.64. Notably, the expansion of the fundamental mode for $\alpha = 2°$ surpasses that of $\alpha = 5°$, resulting in a reduced beam divergence and a higher η.

In Fig. 4(b), we present the variation in η as a function of the vertical length of the tapered portion. As this length increases, the tapering angle decreases, and the fundamental mode continues to expand. These effects collectively contribute to a reduction in far-field divergence, ultimately enabling more efficient light collection. In addition, we overlaid the measured heights of Ga-polar and N-polar NWs [as shown in Fig. 2(d)] in Fig. 4(b). The combination of simulation and experimental data underscores the substantial potential for achieving ultralong NWs with a notably high extraction efficiency through the utilization of N-polar NWs.

To examine the relationship between the diameter of the NW and light extraction properties, the NW diameter was systematically varied from 110 to 300 nm. The simulation results, as depicted in Fig. 5(a), reveal the correlation between the effective refractive index n_{eff}, NW diameter d, and photon wavelength λ. Notably, when the NW diameter is approximately $d/\lambda \approx 0.38$ or lower, the NW exclusively supports the fundamental HE_{11} mode. However, as the NW radius increases, a greater number of higher-order modes (specifically TE_{01} and TM_{01}) become observable. Figure 5(b) illustrates the dependence of η on d/λ, while Fig. 5(c) displays the ratio of the guided emission to the leaked emission as d/λ varies for two distinct substrates. Our simulation outcomes indicate that, for diameters smaller than 0.25λ, η remains exceedingly low due to the absence of guided modes—a finding consistent with the relationship depicted in Fig. 5(a). Beyond this point, η exhibits an upward trend with increasing diameter, reaching its peak at $d/\lambda = 0.38$. A further increase in diameter prompts the dominance of higher-order leaky modes in the waveguide, leading to light coupling with these modes, as corroborated by Fig. 5(a). Consequently, the emission ratio declines, yielding a further decrease in η. These findings underscore the critical role of NW diameter control in achieving high η. In addition, we superimposed the measured diameters of

FIG. 5. (a) Effective refractive indices of first three guided modes as a function of diameter/wavelength. Variation in (b) the light extraction efficiency at the NW end and (c) the ratio of the transmitted power coupled to guided modes and leaky modes as a function of diameter/wavelength for two different substrates, GaN and Au.

Ga-polar and N-polar NWs [as shown in Fig. 2(e)] in Fig. 5(b). The synergy between these experimental and simulation results suggests that a shift to N-polar NWs yields an enhanced extraction efficiency. Moreover, a substantial increase in η is observed upon changing the substrate from GaN to Au. This effect is attributed to the redirection of half of the emitted photons downward from the dipole, and the incorporation of a gold mirror at the base effectively reflects a reasonable portion of these photons back into the waveguide, facilitating coupling with the fundamental mode. Notably, the successful transfer of NWs between substrates has experimentally been demonstrated.[57]

In conclusion, we have demonstrated SAE of GaN NWs with embedded InGaN Qdisks on GaN templates with both Ga- and N-polarities. It is observed that N-polar NWs exhibit better control over shape and geometry, which is beneficial for optical waveguiding. The optical properties of the Qdisks were evaluated using CL and PL, revealing that N-polar Qdisks have a peak emission at a higher wavelength due to increased indium incorporation, while the Ga-polar Qdisks show a bimodal distribution due to higher indium inhomogeneities. Our theoretical findings, presented here and complemented by experimental results, unequivocally underscore the potential of N-polar NWs in achieving highly efficient quantum emitters. Although the minimal diameter (150 nm) of our Qdisks exceeds the values required for them to act as quantum emitters, there are methods available to convert these Qdisks into QDs through further processing. One such technique involves *in situ* thermal decomposition of the sidewall surfaces followed by ultrahigh subsequent regrowth of an additional GaN capping shell to encapsulate the InGaN/GaN NW QDs.[58] Furthermore, we have provided a detailed single NW-level theoretical analysis that emphasizes the importance of geometry control on the extraction efficiency and emission profile of quantum light sources achievable from N-polar NWs. Hence, our study provides valuable insights into the design and fabrication of III-nitride N-polar NWs with enhanced optical properties, paving the way for advanced quantum technologies.

See the supplementary material for the experimental details of CL and PL measurements, PL emission spectra, and additional CL data.

AUTHOR DECLARATIONS

Conflict of Interest

The authors have no conflicts to disclose.

Author Contributions

Arnob Ghosh: Conceptualization (equal); Formal analysis (lead); Investigation (equal); Methodology (equal); Writing – original draft (lead); Writing – review & editing (lead). **Kamruzzaman Khan**: Investigation (equal); Methodology (equal); Writing – review & editing (supporting). **Shrivatch Sankar**: Formal analysis (supporting); Investigation (supporting). **Zhe (Ashley) Jian**: Investigation (supporting); Methodology (supporting). **Syed M. N. Hasan**: Formal analysis (supporting); Investigation (supporting). **Elaheh Ahmadi**: Funding acquisition (equal); Resources (equal); Supervision (equal); Writing – review & editing (supporting). **Shamsul Arafin**: Conceptualization (equal); Funding acquisition (equal); Resources (equal); Supervision (equal); Writing – original draft (supporting); Writing – review & editing (lead).

DATA AVAILABILITY

The data that support the findings of this study are available within the article and its supplementary material.

REFERENCES

[1] S. Arafin, X. Liu, and Z. Mi, "Review of recent progress of III-nitride nanowire lasers," J. Nanophotonics **7**(1), 074599 (2013).

[2] M. G. Kibria, J. P. Edwards, C. M. Gabardo, C.-T. Dinh, A. Seifitokaldani, D. Sinton, and E. H. Sargent, "Electrochemical CO_2 reduction into chemical feedstocks: From mechanistic electrocatalysis models to system design," Adv. Mater. **31**(31), 1807166 (2019).

[3] M. G. Kibria, F. A. Chowdhury, S. Zhao, B. AlOtaibi, M. L. Trudeau, H. Guo, and Z. Mi, "Visible light-driven efficient overall water splitting using *p*-type metal-nitride nanowire arrays," Nat. Commun. **6**(1), 6797 (2015).

[4] Y. P. Huang, W. C. Hsu, H. Y. Liu, and C. S. Lee, "Enhancement-mode tri-gate nanowire InAlN/GaN MOSHEMT for power applications," IEEE Electron Device Lett. **40**(6), 929–932 (2019).

[5] J. Teubert, P. Becker, F. Furtmayr, and M. Eickhoff, "GaN nanodiscs embedded in nanowires as optochemical transducers," Nanotechnology **22**(27), 275505 (2011).

[6] K. Maier, A. Helwig, G. Müller, J. Schörmann, and M. Eickhoff, "Photoluminescence detection of surface oxidation processes on InGaN/GaN nanowire arrays," ACS Sens. **3**(11), 2254–2260 (2018).

[7] E. Calleja, M. A. Sánchez-García, F. J. Sánchez, F. Calle, F. B. Naranjo, E. Muñoz, U. Jahn, and K. Ploog, "Luminescence properties and defects in GaN nanocolumns grown by molecular beam epitaxy," Phys. Rev. B **62**(24), 16826–16834 (2000).

[8] J. Ristić, E. Calleja, S. Fernández-Garrido, L. Cerutti, A. Trampert, U. Jahn, and K. H. Ploog, "On the mechanisms of spontaneous growth of III-nitride nanocolumns by plasma-assisted molecular beam epitaxy," J. Cryst. Growth **310**(18), 4035–4045 (2008).

[9] R. Calarco, R. J. Meijers, R. K. Debnath, T. Stoica, E. Sutter, and H. Lüth, "Nucleation and growth of GaN nanowires on Si(111) performed by molecular beam epitaxy," Nano Lett. **7**(8), 2248–2251 (2007).

[10] J. Deng, J. Yu, Z. Hao, J. Kang, B. Lu, L. Wang, C. Sun, Y. Han, B. Xiong, J. Wang, H. Li, and Y. Luo, "Disk-shaped GaN quantum dots embedded in AlN nanowires for room-temperature single-photon emitters applicable to quantum information technology," ACS Appl. Nano Mater. **5**(3), 4000–4008 (2022).

[11] E. Chernysheva, Ž. Gačević, N. García-Lepetit, H. P. van der Meulen, M. Müller, F. Bertram, P. Veit, A. Torres-Pardo, J. M. González Calbet, J. Christen, E. Calleja, J. M. Calleja, and S. Lazić, "Blue-to-green single photons from InGaN/GaN dot-in-a-nanowire ordered arrays," Europhys. Lett. **111**(2), 24001 (2015).

[12] S. Kremling, C. Tessarek, H. Dartsch, S. Figge, S. Höfling, L. Worschech, C. Kruse, D. Hommel, and A. Forchel, "Single photon emission from InGaN/GaN quantum dots up to 50 K," Appl. Phys. Lett. **100**(6), 061115 (2012).

[13] M. J. Holmes, K. Choi, S. Kako, M. Arita, and Y. Arakawa, "Room-temperature triggered single photon emission from a III-nitride site-controlled nanowire quantum dot," Nano Lett. **14**(2), 982–986 (2014).

[14]P. K. Saha, K. S. Rana, N. Thakur, B. Parvez, S. A. Bhat, S. Ganguly, and D. Saha, "Room temperature single-photon emission from InGaN quantum dot ordered arrays in GaN nanoneedles," Appl. Phys. Lett. **121**(21), 211101 (2022).

[15]J. L. O'Brien, A. Furusawa, and J. Vučković, "Photonic quantum technologies," Nat. Photonics **3**(12), 687–695 (2009).

[16]J.-Y. Hu, B. Yu, M.-Y. Jing, L.-T. Xiao, S.-T. Jia, G.-Q. Qin, and G.-L. Long, "Experimental quantum secure direct communication with single photons," Light: Sci. Appl. **5**(9), e16144 (2016).

[17]T. E. Northup and R. Blatt, "Quantum information transfer using photons," Nat. Photonics **8**(5), 356–363 (2014).

[18]W. Guo, M. Zhang, A. Banerjee, and P. Bhattacharya, "Catalyst-free InGaN/GaN nanowire light emitting diodes grown on (001) silicon by molecular beam epitaxy," Nano Lett. **10**(9), 3355–3359 (2010).

[19]V. Consonni, M. Knelangen, U. Jahn, A. Trampert, L. Geelhaar, and H. Riechert, "Effects of nanowire coalescence on their structural and optical properties on a local scale," Appl. Phys. Lett. **95**(24), 241910 (2009).

[20]M. Yoshizawa, A. Kikuchi, M. Mori, N. F. Nobuhiko Fujita, and K. K. Katsumi Kishino, "Growth of self-organized GaN nanostructures on Al$_2$O$_3$(0001) by RF-radical source molecular beam epitaxy," Jpn. J. Appl. Phys. **36**(4B), L459 (1997).

[21]E. Calleja, M. Sánchez-García, F. Sánchez, F. Calle, F. Naranjo, E. Munoz, S. Molina, A. Sanchez, F. Pacheco, and R. García, "Growth of III-nitrides on Si(111) by molecular beam epitaxy doping, optical, and electrical properties," J. Cryst. Growth **201–202**, 296–317 (1999).

[22]H. P. T. Nguyen, S. Zhang, K. Cui, X. Han, S. Fathololoumi, M. Couillard, G. A. Botton, and Z. Mi, "p-type modulation doped InGaN/GaN dot-in-a-wire white-light-emitting diodes monolithically grown on Si(111)," Nano Lett. **11**(5), 1919–1924 (2011).

[23]C. F. Lin, J. H. Zheng, Z. J. Yang, J. J. Dai, D. Y. Lin, C. Y. Chang, Z. X. Lai, and C. S. Hong, "High-efficiency InGaN-based light-emitting diodes with nanoporous GaN:Mg structure," Appl. Phys. Lett. **88**(8), 083121 (2006).

[24]K. Kishino, A. Kikuchi, H. Sekiguchi, and S. Ishizawa, "InGaN/GaN nanocolumn LEDs emitting from blue to red," Proc. SPIE **6473**, 64730T (2007).

[25]H.-W. Lin, Y.-J. Lu, H.-Y. Chen, H.-M. Lee, and S. Gwo, "InGaN/GaN nanorod array white light-emitting diode," Appl. Phys. Lett. **97**(7), 073101 (2010).

[26]A. Roshko, M. Brubaker, P. Blanchard, T. Harvey, and K. A. Bertness, "Selective area growth and structural characterization of GaN nanostructures on Si(111) substrates," Crystals **8**(9), 366 (2018).

[27]Ž. Gačević, D. Gómez Sánchez, and E. Calleja, "Formation mechanisms of GaN nanowires grown by selective area growth homoepitaxy," Nano Lett. **15**(2), 1117–1121 (2015).

[28]J. Kamimura, K. Kishino, and A. Kikuchi, "Dislocation reduction via selective-area growth of InN accompanied by lateral growth by rf-plasma-assisted molecular-beam epitaxy," Appl. Phys. Lett. **97**(14), 141913 (2010).

[29]T. Schumann, T. Gotschke, F. Limbach, T. Stoica, and R. Calarco, "Selective-area catalyst-free MBE growth of GaN nanowires using a patterned oxide layer," Nanotechnology **22**(9), 095603 (2011).

[30]K. Tomioka, T. Tanaka, S. Hara, K. Hiruma, and T. Fukui, "III–V nanowires on Si substrate: Selective-area growth and device applications," IEEE J. Sel. Top. Quantum Electron. **17**(4), 1112–1129 (2011).

[31]M. Sobanska, Z. R. Zytkiewicz, K. Klosek, R. Kruszka, K. Golaszewska, M. Ekielski, and S. Gieraltowska, "Selective area formation of GaN nanowires on GaN substrates by the use of amorphous Al$_x$O$_y$ nucleation layer," Nanotechnology **31**(18), 184001 (2020).

[32]C. H. Wu, P. Y. Lee, K. Y. Chen, Y. T. Tseng, Y. L. Wang, and K. Y. Cheng, "Selective area growth of high-density GaN nanowire arrays on Si(111) using thin AlN seeding layers," J. Cryst. Growth **454**, 71–81 (2016).

[33]S. M. N. Hasan, W. You, A. Ghosh, S. M. Sadaf, and S. Arafin, "Selective area epitaxy of GaN nanostructures: MBE growth and morphological analysis," Cryst. Growth Des. **23**(6), 4098–4104 (2023).

[34]A. Uedono, K. Shojiki, K. Uesugi, S. F. Chichibu, S. Ishibashi, M. Dickmann, W. Egger, C. Hugenschmidt, and H. Miyake, "Annealing behaviors of vacancy-type defects in AlN deposited by radio-frequency sputtering and metalorganic vapor phase epitaxy studied using monoenergetic positron beams," J. Appl. Phys. **128**(8), 085704 (2020).

[35]D. N. Nath, E. Gür, S. A. Ringel, and S. Rajan, "Growth model for plasma-assisted molecular beam epitaxy of N-polar and Ga-polar In$_x$Ga$_{1−x}$N," J. Vac. Sci. Technol. B **29**(2), 021206 (2011).

[36]K. Khan, S. Diez, K. Sun, C. Wurm, U. K. Mishra, and E. Ahmadi, "Observation of self-assembled InGaN/GaN superlattice structure grown on N-polar GaN by plasma-assisted molecular beam epitaxy," APL Mater. **9**(12), 121114 (2021).

[37]K. Khan, Z. Jian, J. Li, K. Sun, and E. Ahmadi, "Selective-area growth of GaN and AlGaN nanowires on N-polar GaN templates with 4° miscut by plasma-assisted molecular beam epitaxy," J. Cryst. Growth **611**, 127181 (2023).

[38]X. Liu, Y. Sun, Y. Malhotra, A. Pandey, P. Wang, Y. Wu, K. Sun, and Z. Mi, "N-polar InGaN nanowires: Breaking the efficiency bottleneck of nano and micro LEDs," Photonics Res. **10**(2), 587–593 (2022).

[39]F. Akyol, D. N. Nath, S. Krishnamoorthy, P. S. Park, and S. Rajan, "Suppression of electron overflow and efficiency droop in N-polar GaN green light emitting diodes," Appl. Phys. Lett. **100**(11), 111118 (2012).

[40]N. H. Tran, B. H. Le, S. Zhao, and Z. Mi, "On the mechanism of highly efficient p-type conduction of Mg-doped ultra-wide-bandgap AlN nanostructures," Appl. Phys. Lett. **110**(3), 032102 (2017).

[41]Y. Wu, D. A. Laleyan, Z. Deng, C. Ahn, A. F. Aiello, A. Pandey, X. Liu, P. Wang, K. Sun, E. Ahmadi, Y. Sun, M. Kira, P. K. Bhattacharya, E. Kioupakis, and Z. Mi, "Controlling defect formation of nanoscale AlN: Toward efficient current conduction of ultrawide-bandgap semiconductors," Adv. Electron. Mater. **6**(9), 2000337 (2020).

[42]M. D. Brubaker, S. M. Duff, T. E. Harvey, P. T. Blanchard, A. Roshko, A. W. Sanders, N. A. Sanford, and K. A. Bertness, "Polarity-controlled GaN/AlN nucleation layers for selective-area growth of GaN nanowire arrays on Si(111) substrates by molecular beam epitaxy," Cryst. Growth Des. **16**(2), 596–604 (2016).

[43]A. Roshko, M. Brubaker, P. Blanchard, T. Harvey, and K. Bertness, "The role of Si in GaN/AlN/Si(111) plasma assisted molecular beam epitaxy: Polarity and inversion," Jpn. J. Appl. Phys. **58**(SC), SC1050 (2019).

[44]A. Roshko, M. D. Brubaker, P. T. Blanchard, T. E. Harvey, and K. A. Bertness, "Eutectic formation, V/III ratio, and controlled polarity inversion in nitrides on silicon," Phys. Status Solidi B **257**(4), 1900611 (2020).

[45]M. D. Brubaker, I. Levin, A. V. Davydov, D. M. Rourke, N. A. Sanford, V. M. Bright, and K. A. Bertness, "Effect of AlN buffer layer properties on the morphology and polarity of GaN nanowires grown by molecular beam epitaxy," J. Appl. Phys. **110**(5), 053506 (2011).

[46]A. Urban, J. Malindretos, J. H. Klein-Wiele, P. Simon, and A. Rizzi, "Corrigendum: Ga-polar GaN nanocolumn arrays with semipolar faceted tips (2013 New J. Phys. 15 053045)," New J. Phys. **16**(1), 019501 (2014).

[47]V. Jindal and F. Shahedipour-Sandvik, "Theoretical prediction of GaN nanostructure equilibrium and nonequilibrium shapes," J. Appl. Phys. **106**(8), 083115 (2009).

[48]J. E. Northrup and J. Neugebauer, "Theory of GaN (10$\bar{1}$0) and (11$\bar{2}$0) surfaces," Phys. Rev. B **53**(16), R10477–R10480 (1996).

[49]X. J. Chen, G. Perillat-Merceroz, D. Sam-Giao, C. Durand, and J. Eymery, "Homoepitaxial growth of catalyst-free GaN wires on N-polar substrates," Appl. Phys. Lett. **97**(15), 151909 (2010).

[50]S. M. N. Hasan, A. Ghosh, S. M. Sadaf, and S. Arafin, "Effects of InGaN quantum disk thickness on the optical properties of GaN nanowires," J. Cryst. Growth **588**, 126654 (2022).

[51]S. Y. Woo, N. Gauquelin, H. P. T. Nguyen, Z. Mi, and G. A. Botton, "Interplay of strain and indium incorporation in InGaN/GaN dot-in-a-wire nanostructures by scanning transmission electron microscopy," Nanotechnology **26**(34), 344002 (2015).

[52]H. K. Cho, J. Y. Lee, N. Sharma, C. J. Humphreys, G. M. Yang, C. S. Kim, J. H. Song, and P. W. Yu, "Effect of growth interruptions on the light emission and indium clustering of InGaN/GaN multiple quantum wells," Appl. Phys. Lett. **79**(16), 2594–2596 (2001).

[53]H. K. Cho, J. Y. Lee, J. H. Song, P. W. Yu, G. M. Yang, and C. S. Kim, "Influence of strain-induced indium clustering on characteristics of InGaN/GaN multiple quantum wells with high indium composition," J. Appl. Phys. **91**(3), 1104–1107 (2002).

[54] M. Kurouchi, T. Araki, H. Naoi, T. Yamaguchi, A. Suzuki, and Y. Nanishi, "Growth and properties of In-rich InGaN films grown on (0001) sapphire by RF-MBE," Phys. Status Solidi B **241**(12), 2843–2848 (2004).

[55] S. Fernández-Garrido, J. Lähnemann, C. Hauswald, M. Korytov, M. Albrecht, C. Chèze, C. Skierbiszewski, and O. Brandt, "Comparison of the luminous efficiencies of Ga- and N-polar $In_xGa_{1-x}N/In_yGa_{1-y}N$ quantum wells grown by plasma-assisted molecular beam epitaxy," Phys. Rev. Appl. **6**(3), 034017 (2016).

[56] C. Chèze, M. Siekacz, G. Muzioł, H. Turski, S. Grzanka, M. Kryśko, J. L. Weyher, M. Boćkowski, C. Hauswald, J. Lähnemann, O. Brandt, M. Albrecht, and C. Skierbiszewski, "Investigation on the origin of luminescence quenching in N-polar (In,Ga)N multiple quantum wells," J. Vac. Sci. Technol. B **31**(3), 03C130 (2013).

[57] M. E. Reimer, G. Bulgarini, N. Akopian, M. Hocevar, M. B. Bavinck, M. A. Verheijen, E. P. A. M. Bakkers, L. P. Kouwenhoven, and V. Zwiller, "Bright single-photon sources in bottom-up tailored nanowires," Nat. Commun. **3**(1), 737 (2012).

[58] X. Sun, P. Wang, B. Sheng, T. Wang, Z. Chen, K. Gao, M. Li, J. Zhang, W. Ge, Y. Arakawa, B. Shen, M. Holmes, and X. Wang, "Single-photon emission from a further confined InGaN/GaN quantum disc via reverse-reaction growth," Quantum Eng. **1**(3), e20 (2019).

22 February 2024 18:43:05